Advanced Industrial and Engineering Polymer Research 1 (2018) 82–92

Contents lists available at ScienceDirect

Advanced Industrial and Engineering Polymer Research

journal homepage: http://www.keaipublishing.com/aiepr

Investigation of interfacial strength parameters in polymer matrix composites: Compatibility and reproducibility

Serge Zhandarov [a, b], Edith Mäder [a, *], Christina Scheffler [a], Gerhard Kalinka [c], Claudia Poitzsch [d], Stefan Fliescher [d]

[a] Leibniz-Institut für Polymerforschung Dresden e.V., Hohe Str. 6, D-01069 Dresden, Germany
[b] "V. A. Bely" Metal-Polymer Research Institute, National Academy of Sciences of Belarus, Kirov Str. 32a, 246050 Gomel, Belarus
[c] BAM Federal Institute for Materials Research and Testing, Unter den Eichen 87, D-12205 Berlin, Germany
[d] Textechno Herbert Stein GmbH & Co. KG, Dohrweg 65, 41066 Mönchengladbach, Germany

ARTICLE INFO

Article history:
Received 26 April 2018
Received in revised form
15 June 2018
Accepted 20 June 2018

Keywords:
Polymer matrix composites
Pull-out test
Local interfacial shear strength
Critical energy release rate
Geometrical factors
Analysis of force-displacement curves

ABSTRACT

Effects of various geometrical and physical factors, as well as the method of data reduction (analysis of experimental force–displacement curves) on the values of local interfacial strength parameters (local IFSS, τ_d, and critical energy release rate, G_{ic}) determined by means of a single fiber pull-out test are discussed. Experimental results of our pull-out tests on several fiber–polymer matrix systems showed that τ_d and G_{ic} weakly depended on geometrical factors. However, the pull-out test appeared to be sensitive to the conditions of specimen formation and testing, such as changing the nature of the contacting surfaces (fiber sizing) and the fiber pull-out rate. Of several methods of τ_d and G_{ic} determination from a force–displacement curve, the most reliable and reproducible one is the approach based on the values of the maximum force recorded in a pull-out test and the interfacial frictional force immediately after fiber debonding.

1. Introduction

Of all micromechanical techniques for determining the interfacial bond strength between fibers and matrices, the pull-out test [1–4] is probably the most popular one. In this test, a fiber is immersed in a matrix droplet fixed by a support such as a flat solid plate [5] (Fig. 1), two thick support fibers (three-fiber test) [6], or specially designed ring [3,6], and after matrix curing or consolidation, the fiber is pulled out of the matrix, and the applied force, F, is recorded as a function of the displacement of the loaded fiber end, s.

Traditionally, the popularity of the pull-out test is accounted for its versatility (it can be successfully applied to a wide range of fiber–matrix systems), experimental simplicity, well-defined test geometry and good reproducibility of experimental results [6,7]. We can agree with the first three points (if the three-fiber test with intricate specimen shape is excluded from the consideration), but reproducibility has always been rather wishful thinking than established fact. For instance, the results obtained within a round-robin program specially undertaken to assess the compatibility of different micromechanical tests and the reproducibility of experimentally measured values of interfacial parameters showed that "the scatter within each laboratory was acceptable but the scatter between laboratories for a particular test was high" [8]. The difference between the IFSS values determined by means of the pull-out test for the same system (carbon fiber + epoxy resin) but at three different laboratories reached as much as 60%! The authors of [8] specified several sources of errors which could affect the measured IFSS values: the accuracy of the measurements of the fiber diameter and embedded length; alignment of the fiber with the loading axis; loading rate; and, the last but not the least, the method of data reduction. It is well known that the apparent interfacial shear strength, defined as [6,9].

$$\tau_{app} = \frac{F_{\max}}{\pi d_f l_e}, \quad (1)$$

* Corresponding author.
E-mail addresses: serge.zhandarov@gmail.com (S. Zhandarov), emaeder@ipfdd.de (E. Mäder), scheffler@ipfdd.de (C. Scheffler), gerhard.kalinka@bam.de (G. Kalinka), c.poitzsch@textechno.com (C. Poitzsch), s.fliescher@textechno.com (S. Fliescher).

https://doi.org/10.1016/j.aiepr.2018.06.002

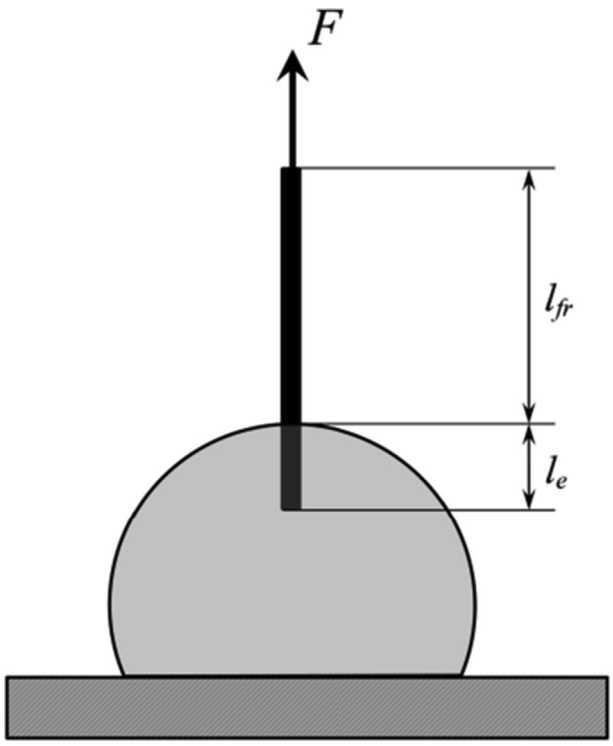

Fig. 1. Scheme of fiber embedding for the pull-out test.

where d_f is the fiber diameter and l_e is the embedded length, strongly depends on the embedded length [4,6] and is not fully due to interfacial adhesion but can include a substantial frictional contribution [10]. Therefore, the main objective of the data reduction is to determine *local* interfacial strength parameters, such as the local IFSS, τ_d [6,11], or the critical energy release rate for interfacial debonding, G_{ic} [10,12,13], from a recorded force–displacement curve, $F = F(s)$. A typical $F(s)$ curve is shown in Fig. 2. Its detailed analysis has been presented elsewhere [14].

Here we would like to highlight the important points in this curve: *A*, the debond point, corresponding to interfacial crack initiation (start of debonding), which manifests itself as a 'kink' (abrupt slope change); *B*, the peak point, at which the measured force reaches its maximum value, $F_{\max}$ (for many force–displacement curves, $F_{\max}$ can be much greater than the debond force, F_d); *C*, the instability

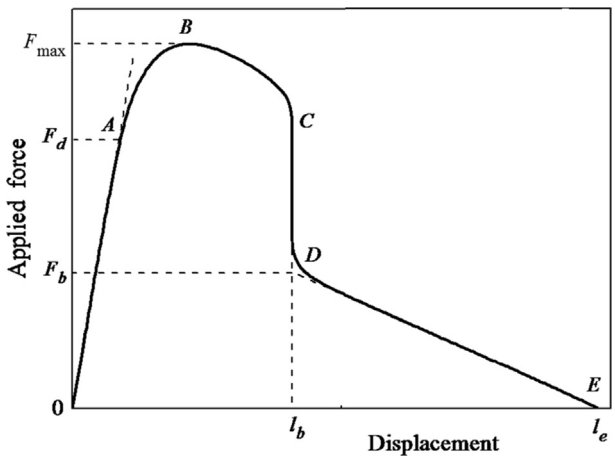

Fig. 2. An idealized force–displacement curve in the pull-out test (for details, see Introduction).

point, at which crack propagation becomes instable; *D*, the point of full debonding (after this point, the $F(s)$ behavior is controlled by frictional interaction between the fiber and the matrix); and *E*, the point of pull-out completion ($s = l_e$).

Generally speaking, we can distinguish the following groups of factors which can affect the IFSS value determined in a pull-out test:

1) Geometrical factors. These include the matrix droplet shape (cylinder/ellipsoid/brick/other) and dimensions; the fiber embedded length and diameter; the free fiber length, l_{fr} (see Fig. 1). The significance of the latter is often neglected, but the experience has shown that l_{fr} can be very important. If it is increased, the slope change at point *A* gets smaller, so that for large free fiber lengths the 'kink' can become visually indistinguishable. In addition, for large l_{fr}, considerable amount of elastic energy can be stored in the fiber near the peak applied load. As a result, segment *BC*, the stable segment with decreasing recorded load, shortens or even vanishes (point *C* gets closer to point *B* and finally coincides with it), and the pull-out test switches from "displacement-controlled" mode to "stress-controlled".
2) Thermodynamic and kinetic factors, first of all, the temperature of specimen formation and the test temperature. The thermal history can also be important; for instance, different specimen cooling rates "freeze" different molecular configurations at the interface/interphase, thus affecting interfacial adhesion and the measured IFSS. This effect is especially pronounced for semi-crystalline thermoplastic polymers [15]. The effect of humidity condition of fabrication [16,17] and testing [18] was also reported. And, finally, the loading rate can also be considered as a kinetic factor, since the interfacial fracture is determined by molecular kinetics (thermal fluctuation theory) [19,20].
3) Theoretical models used for data reduction. These can be divided into two large groups, "stress-based" [6,11] and "energy-based" [10,12,13], depending of the parameter which is chosen as a debonding criterion (τ_d or G_{ic}). Then, different models have been developed within each group, which means different equations relating interfacial strength parameters to force values reached at the important points of the force–displacement curve (*A*, *B*, *D*). And, finally, the choice of points used for τ_d or G_{ic} calculation is also important; according to it, we distinguish between "traditional" approach (τ_d or G_{ic} from F_d [10,12,21,22]), "alternative" approach (interfacial parameters from F_b and $F_{\max}$ [23,24]), and "indirect" approach (from $F_{\max}$ as a function of the embedded length in a wide l_e range [11,25]). Since the experimental pull-out procedure is not ideal, the values of interfacial strength parameters obtained using these approaches may differ. Their comparison could help to decide which approach is the most adequate for interface strength characterization. Note that in this paper we will not consider dynamic crack growth. In pull-out and microbond tests, it takes place only at the instable, essentially non-equilibrium stage (*CD* in Fig. 2) which is not important in most theoretical models, in contrast to the tapered double cantilever beam (TDCB) test [26–28]. At previous, quasi-static stages of the pull-out and microbond tests, the kinetic energy inside the specimen is negligible, and the energy-based and stress-based approaches can be considered as nearly equivalent [29].

For several decades, two research teams, one at the Leibniz-Institut für Polymerforschung Dresden e.V. (IPF) and the other at the Federal Institute for Materials Research and Testing in Berlin (BAM) are preferably using, besides other micromechanical tests, single fiber pull-out tests for interface strength characterization in fiber–matrix systems. In essence, the tests employed in the two

institutions are very similar. However, there are also smaller or larger differences, e.g., in matrix droplet radius, loading rate, free fiber length, and data treatment.

The aim of this paper was to perform the pull-out test on several identical fiber–matrix systems in parallel at both institutions and then assess how these differences affect the measured values of the interfacial strength parameters. Additionally, the influence of the theoretical approach used for τ_d and G_{ic} calculation was studied.

2. Experimental

2.1. Materials and treatments

2.1.1. Fibers

The glass fibers (GF) were manufactured at the IPF using a continuous spinning equipment. The fiber diameter varied from 10 to 15 μm. A part of fibers was sized with 1 wt% γ-aminopropyltriethoxysilane (APS) or with APS and epoxy-based film former (APS+EP) immediately after cooling in the continuous spinning process. Both unsized and γ-APS sized fibers were then used for the fabrication of pull-out specimens, which included fiber embedding in the matrix droplet to a preset length (using an equipment described in Ref. [30] followed by the matrix curing as described below.

The carbon fibers were provided by Toho Tenax as treated and epoxy-sized HT-fibers (HTA40 E13) which were desized by CO_2-plasma. The fiber diameter varied from 6 to 8 μm.

2.1.2. Epoxy resin matrices

Three epoxy-based matrices were used for the specimens fabrication. One was a hot curing anhydride hardening system (manufactured by Ciba Specialty Chemicals) consisting of epoxy resin Araldite LY 556, anhydride hardener HY 917, and imidazole accelerator DY 070 in a weight ratio of 100:90:1. After embedding a fiber in the matrix droplet, it was cured for 3 h at 95 °C and then for 4 h at 128 °C. The glass transition temperature for this resin, measured by means of differential scanning calorimetry at a constant heating rate of 10 K/min, was 137 °C. The second matrix was hot curing amino hardening system (also manufactured by Ciba Specialty Chemicals). It contained epoxy resin Araldite LY 556 and cycloaliphatic polyamine hardener Aradur 22962 in a weight ratio 100:23. The resin mixture was heated up to 80 °C in 30 s, followed by embedding the fiber and heating up to 128 °C in 2 min. The curing process was 15 min at 128 °C followed by 2 h at 160 °C. The measured glass transition temperature for this resin was 141 °C. The third matrix was also a hot curing amino hardening system RIM 135/RIM 137 in a weight ratio 100:30 (manufactured by Momentive Specialty Chemicals, Ohio, USA). After embedding a fiber in the matrix droplet at 45 °C, the temperature was increased to 85 °C and it was cured at this temperature for 60 min. Afterwards it was cooled to ambient temperature and after collecting all specimens treated in an oven at 80 °C for 6 h.

2.1.3. Polyamide 6.6 matrix

A droplet of Ultramid A27 (manufactured by BASF, Ludwigshaven, Germany) was heated up on the sample carrier in a closed module to 80 °C, flashed for 30 min at 80 °C and heated to 290 °C. Then, a fiber was embedded in the droplet to a depth of 80–200 μm. The specimen kept for 30 s at 290 °C and then cooled to ambient temperature.

The mechanical and thermal properties of the fibers and matrices, required for the calculation of interfacial strength parameters, are listed in Table 1.

2.2. Pull-out testing—IPF lab equipment

Specimens were made using a self-made sample preparation equipment designed and constructed earlier at the IPF [31]. A small amount of the epoxy resin mixture was placed into a special aluminum carrier to form a sitting droplet with nearly hemispherical crowned part. Two video cameras placed under optimized angles enabled to exactly visualize the position of the single glass fiber to be embedded. Fibers were end-embedded into the epoxy resin mixture perpendicularly, to a PC-controlled preselected embedded length in the range of 50–150 μm [32]. Then the specimens were cured in the embedding device on the top of a micro-heater under conditions stated above in Subsection 2.1. The arrangement of the embedded fiber in the pull-out equipment is presented in Fig. 3a.

The pull-out apparatus [32] allowed investigators to perform pull-out tests at “slow” (0.01 μm/s) and “fast” (1 μm/s) displacement rates under controlled conditions (23 °C, 50% relative humidity). The force–displacement curves were recorded in a PC at the data acquisition rate 1 s^{-1}. The free fiber lengths were kept as short as possible (<50 μm), and the installation was stiff enough to discern the “kinks” in the force–displacement curves, which indicated the onset of debonding. Diameters of the fibers were measured immediately after pull-out testing using an optical microscope. At least 15 specimens were tested for each fiber–matrix combination.

2.3. Pull-out testing — FIMATEST

Here a commercially available pull-out test [33] is presented as a micromechanical technique to determine the interfacial interaction between fibers and matrices and is compared with the results

Table 1
Fiber and matrix properties and specimen dimensions.

Property	Glass fiber	Carbon fiber	Epoxy 1[a]	Epoxy 2[b]	Epoxy 3[c]	PA6.6
Fiber diameter, d_f (μm)	10…15	6…8	—	—	—	—
Radius of the matrix droplet, R_m (mm)	—	—	1.25 (IPF, Textechno); 0.50 (BAM)		1.25	1.25
Axial tensile modulus, E_A (GPa)	75	240	3.2	2.88	2.9	3.2
Transverse tensile modulus, E_T (GPa)	75	24	3.2	2.88	2.9	3.2
Axial Poisson ratio, ν_A	0.17	0.2	0.35	0.35[c]	0.35	0.3
Transverse Poisson ratio, ν_T	0.17	0.2[d]	0.35	0.35[c]	0.35	0.3
Axial CTE, α_A (K^{-1})	5×10^{-6}	-0.1×10^{-6}	57×10^{-6}	57×10^{-6}[d]	50×10^{-6}[d]	81×10^{-6}[d]
Transverse CTE, α_T (K^{-1})	5×10^{-6}	18×10^{-6}[d]	57×10^{-6}	57×10^{-6}[d]	50×10^{-6}[d]	81×10^{-6}[d]
Stress-free temperature, °C	—	—	128	141	89	65
Embedded fiber length, l_e (μm)	10[e]…140	80…200	—	—	—	—

[a] Araldite LY556 epoxy/HY917 hardener/DY070 accelerator in weight ratio 100:90:1.
[b] Araldite LY556 epoxy/Aradur 22962 hardener in weight ratio 100:23.
[c] RIM 135 epoxy/RIM 137 hardener in weight ratio 100:30.
[d] Estimated values.
[e] Specimens with l_e < 40 μm were discarded.

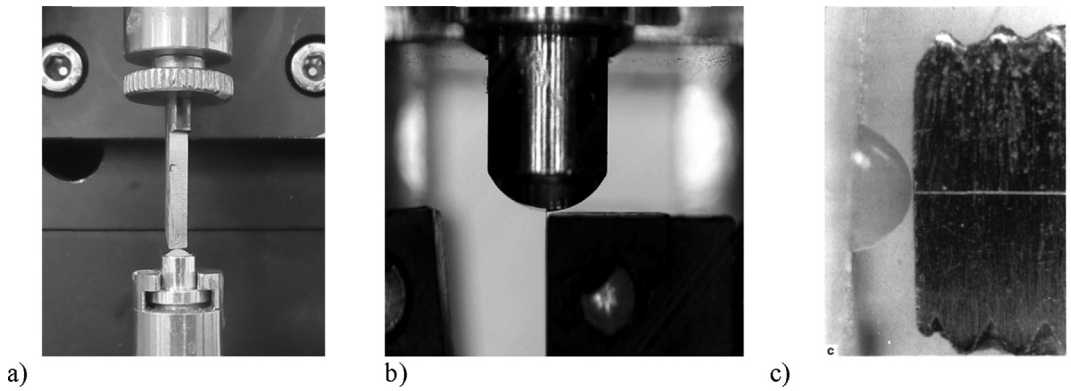

Fig. 3. Arrangement of fiber pull-out in experimental installations: a) IPF, b) Textechno, c) BAM.

determined by using the pull-out tests developed by research institutes. However, this test is not yet standardized. We employ the FIMATEST system [34] developed by Textechno to characterize the fiber–matrix strength parameters through the pull-out test and compare the results with those of lab tests. To prepare the single fiber composite samples the FIMABOND device of the FIMATEST system is used. This is a partially automated embedding station, suitable for all kind of matrices — thermoset, thermoplastic and mineral matrices — and fibers. First, the fiber is approached to the top of the matrix until contact is made. The nominal embedded length is determined by the force that is necessary to fully debond the fiber from the matrix which should not exceed the tensile strength of the fiber leading to fiber failure. Finally, the matrices are cured and consolidated, respectively, as described in Sections 2.1 and 2.2. To process thermoplastics, the sample chamber of the FIMABOND can also be flushed with inert gas, e.g. argon or nitrogen. After preparing the specimens, the sample is ready for pulling-out the fiber at a constant displacement rate of 1.6 μm/s and record the applied forces as a function of displacement.

A special accessory for Textechno's single fiber linear-density and tensile tester FAVIMAT+ is used to perform the pull-out test. The FAVIMAT+ is equipped by a high-resolution load cell (1 μN at 200 cN full range) as well as a highly precise and sturdy mechanics. The cross section of the embedded fiber must be known to fully evaluate the measured data. The cross-sectional area is determined, before embedding and the pull-out test, by the FAVIMAT+ as well.

For the pull-out test, the prepared single fiber composite sample is put upside-down in the direct clamping system of the pull-out device (Fig. 3b). To ensure a precise alignment of the fiber to the jaw faces and the matrix surface, a microscopic camera is integrated in the pull-out device. With the help of the camera, the fiber is adjusted parallel to the clamps and with minimal distance between the jaws and the matrix. Then the pull-out test is started, the force-displacement curve is recorded, and evaluated automatically by the installed software.

2.4. Pull-out testing — BAM lab equipment

An advanced pull-out test device has been used [35] in order to perform a controlled and stable growth of the debonding crack. Piezo translators for the precise generation of the displacement and piezo force sensors were used to guarantee high stiffness. The components are mounted on a highly stiff steel frame. To minimize the energy stored in the test device, the elastic energy stored in the sample has to be also minimized. Therefore, short free fiber lengths in the range of 10–30 μm were used. The free fiber end was fixed with stiff cyano glue, and the amount of polymeric matrix material was minimized. The piezo translator and the high voltage amplifier were supplied by Physic Instruments (Germany), the piezo force sensor and the charge amplifier by Kistler (Switzerland). The load function of the fiber and the resulting force signals were computer controlled via a 12-bit D/A resp. A/D port from Keithley (USA). The computer program for controlling the pull-out test was developed at BAM. It includes a drift compensation of the piezo components, and storage and presentation of the resulting data.

For embedding single fibers in a matrix droplet, a special "embedding machine" has been developed. It allows defined curing of a thermoset droplet having a matrix radius of 0.5 mm by an electric furnace. The embedding of a clamped single fiber into the zenith of the droplet (Fig. 3c) can be controlled by a light microscope. Due to flow of the droplet caused by its weight and shrinkage of the droplet caused by crystallization during cooling or curing, respectively, it is necessary to find out the real embedded length of the fiber in the prepared sample. It is assumed that the displacement where the force becomes zero is equal to the embedded length of the fiber. The displacement rate of the pull-out was kept constant at 1 μm/s.

2.5. Analysis of force–displacement curves

The recorded force–displacement curves were analyzed in a PC in *Mathematica*® programming environment [36] in order to recognize and discard unsuccessful pull-out tests, and to determine the important points required for the calculation of the interfacial strength parameters (see Introduction) in successful curves. This procedure can be illustrated using Fig. 4. First, the recorded force–displacement curve is plotted in *Mathematica*, and its zero level (horizontal asymptote) is determined (Fig. 4a). Then, the curve is replotted (shifted along the vertical axis) so that the force in the asymptote region is zero, and the positions of points *D* and *E* are determined (Fig. 4b; cf. Fig. 2). Displacement *OE* corresponds to complete pull-out and is equal to the embedded length, l_e. It is clearly seen that both points *D* and *E* are easily discernible. However, determination of the position of the point corresponding to debonding onset ("kink" in the ascending part of the force–displacement curve) runs into difficulties. When we consider the whole curve (Fig. 4a and b), it is impossible to point any kink in the ascending segment. On a larger scale (Fig. 4c), one can see that segment *OA* virtually consists of three quasi-linear sections OA_1, A_1A_2 and A_2B, with two kinks, A_1 and A_2 between them. Which of these kinks corresponds to the crack initiation? To achieve better understanding of this problem, it may be instructive to calculate τ_d and τ_f for *both* kinks and also compare the results with the values obtained using the "alternative" method, i.e. from F_b and F_{max} (see

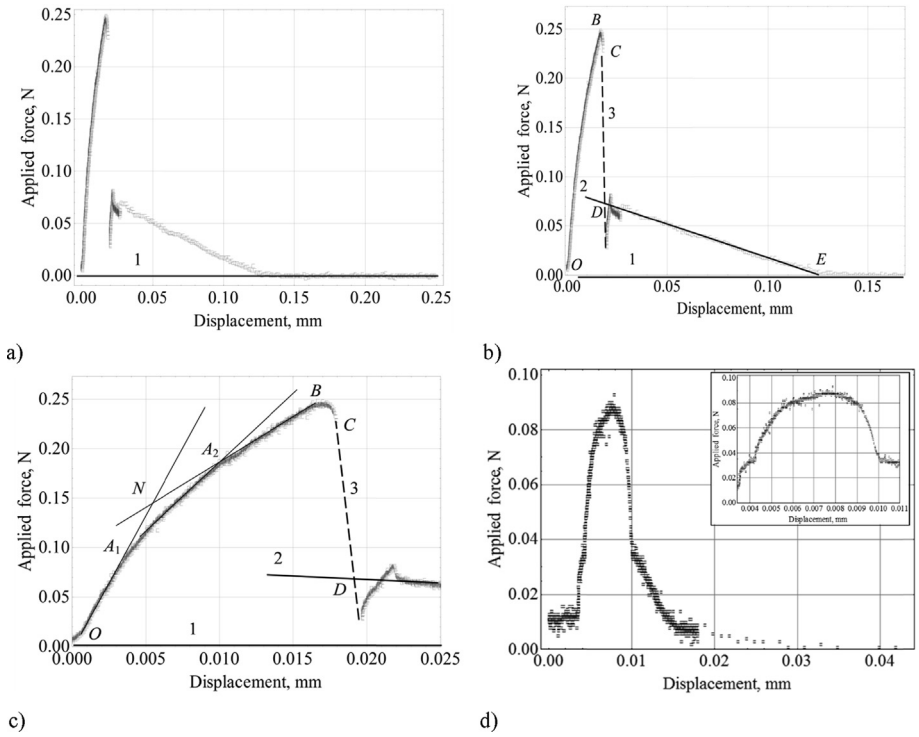

Fig. 4. Analysis of force–displacement curves in the pull-out test (see Subsection 2.5): a) determination of zero level (line 1); b) determination of post-debonding friction (point *D*) and embedded length (point *E*); c) different approaches to finding the point corresponding to crack initiation; d) force–displacement curve for short embedded length.

Section 3). Table 2 illustrates this for the specimen whose force–displacement curves are presented in Fig. 3a–c (γ-APS sized fiber + Epoxy 1).

If we consider A_1 as the kink point, the calculated local IFSS is moderate ($\tau_{d1} = 47.28$ MPa), but the interfacial frictional stress required to reach the experimental F_{max} value at the peak point appeared to be greater than τ_{d1} ($u < 0$ and $\tau_{f1} > \tau_{d1}$), which is physically impossible. With A_2 as the kink point, $\tau_{d2} = 80.40$ MPa and $\tau_{f2} = 34.31$ MPa, which is comparable to the values calculated using the "alternative" approach (99.61 and 13.72 MPa, respectively); however, even in this case the τ_{f2} value looks to be overestimated. Nevertheless, the choice of A_2 is definitely better.

In order to evaluate the force–displacement curves automatically, some experimentalists proposed to consider the point of intersection of two tangent lines (point *N* in Fig. 4c) as a kink. This trick is often used in experimental physics and chemistry in order to estimate the transition point between two physically different processes which contribute to an experimental curve. If one of which starts at some point (here — point *O*), is nearly linear here and contributes nearly 100% to the curve at this point, and the other one takes place far from this point (here — at segment A_2B), is linear at least at the right point of this segment and contributes 100% to the curve here, then the point of intersection of two tangent lines can be conventionally taken as a transition point. However, experimental force–displacement curves recorded in a pull-out test do not fit this pattern. Their left segment (OA_1) is nearly linear indeed and is determined by the intact interface over the whole embedded area (interfacial bonding) which contributes 100% to the measured force. But the right segment (A_2B) does not correspond to any pure other process! It includes substantially non-zero contributions of adhesion and friction over its whole length and even further, up to point *D*! Therefore, it would be a serious mistake to draw a tangent line at point A_2 and consider segment A_2B as "frictional" one. There is only one purely frictional segment in the force–displacement curve, namely, segment *DE* (Fig. 4b). Moreover, as was shown above, choosing the kink point below point A_2 is, in all probability, not correct.

All force–displacement curves recorded in our pull-out tests were similar (and looked like that presented in Fig. 4a–c) for specimens with sufficiently large embedded lengths. For short embedded length, their shapes were different (Fig. 4d). First, the "kinks" in such curves were not discernible at all. Second, the calculated τ_d values for these specimens were extremely high. This may be due to the effect of meniscus which is negligible if l_e is much larger than the length of the meniscus region but can be substantial when these two lengths are comparable. And the other reason may be the fact that the shear-lag analysis is not valid if $l_e < (4\ldots5)d_f$ [12]. Therefore, we excluded such specimens from our consideration. Only specimens with $l_e > 40$ μm (which is about 4 fiber diameters) were taken into account in Table 3.

Table 2
Local IFSS and interfacial frictional stress calculated for one specimen using different methods.

d_f, μm	l_e, μm	F_{max}, N	F_b, N	F_d	τ_{d1}, MPa	τ_{f1}, MPa	τ_{d2}, MPa	τ_{f2}, MPa
13.34	129	0.2487	0.0744	$F(A_1) = 0.0905$ N	47.28	Indeterminate ($>\tau_{d1}$)	99.61	13.72
				$F(A_2) = 0.1875$ N	80.40	34.31		

τ_{d1} and τ_{f1} were calculated using the "traditional" approach (from F_{max} and F_d); τ_{d2} and τ_{f2}, using the "alternative" approach (from F_{max} and F_b).

Table 3
Adhesion strength parameters for glass fiber – LY556 epoxy systems.

Hardener/Treatment	Comment	N	n	τ_{d2}, MPa	τ_{f2}, MPa	τ_{d1}, MPa	τ_{f1}, MPa	G_{ic} (alternative*), J/m^2	τ_d/τ_f (indirect), MPa	G_{ic}/τ_f (indirect), (J/m^2)/MPa
HY 917/–	F	16	10	84.3 ± 8.5	14.1 ± 8.1	64.7 ± 13.5	50.6 ± 10.9	34.6 ± 13.5	84.3/26.6	14.1/32.4
	F-0.5	15	9	55.5 ± 15.8	9.1 ± 2.8	48.3 ± 13.8	38.2 ± 15.9	12.3 ± 3.8	54.7/27.2	5.2/28.4
	S	32	22	73.4 ± 15.3	18.3 ± 9.5	62.0 ± 14.9	43.5 ± 10.4	18.9 ± 9.6	56.6/46.3	2.6/46.0
	BAM	37	25	86.6 ± 15.3	22.5 ± 7.6	69.4 ± 18.7	44.5 ± 17.3	23.7 ± 17.6	92.7/15.5	20.5/22.5
HY 917/APS	F	16	7	113.9 ± 10.7	10.0 ± 6.4	88.7 ± 8.0	77.5 ± 12.4	50.1 ± 13.2	111.9/0.0	7.9/61.6
	S	29	11	87.5 ± 22.0	13.4 ± 6.1	71.8 ± 19.4	55.4 ± 18.8	32.2 ± 19.2	80.8/35.2	8.8/37.6
	BAM	33	13	119.2 ± 17.5	3.9 ± 2.2	97.8 ± 18.1	53.6 ± 20.8	65.2 ± 35.0	102.7/54.4	8.1/55.5
Aradur/–	F	16	15	95.1 ± 18.3	21.6 ± 9.9	81.8 ± 17.1	54.0 ± 15.6	37.9 ± 16.7	94.2/0.0	59.5/6.1
	S	25	22	91.6 ± 13.7	17.6 ± 7.1	78.3 ± 13.6	49.2 ± 9.1	41.3 ± 21.5	77.9/50.0	5.7/50.7
Aradur/APS	F	22	9	138.0 ± 16.4	15.7 ± 8.0	116.7 ± 12.8	80.2 ± 15.4	86.0 ± 28.6	141.4/0.0	32.5/55.6
	S	40	23	129.8 ± 30.5	10.9 ± 4.0	102.9 ± 19.0	77.8 ± 18.1	93.8 ± 47.8	129.8/42.7	51.1/34.8

N — total number of specimens; n — number of "good" specimens.
F — "fast" pull-out (1 μm/s); S — "slow" pull-out (0.01 μm/s); BAM — "fast" pull-out (1 μm/s), matrix radius 0.5 mm. Acquisition rate 1 s^{-1}.
F-0.5 — "fast" pull-out (1 μm/s) with data acquisition rate 2 s^{-1}.
$\{\tau_{d1}, \tau_{f1}\}$ — from F_d and F_{max} ("traditional" method).
$\{\tau_{d2}, \tau_{f2}\}$ — from F_{max} and post-debonding fricrion ("alternative" method).
* Calculated using Eqs. (A6)–(A18), with $\tau_f = \tau_{f2} = F_b/(2\pi\, r_f\, l_e)$ and crack length a corresponding to the peak force $F = F_{max}$.

3. Data reduction: choice and calculation of interfacial strength parameters

In order to determine interfacial strength parameters, we used two substantially different analytical models distinguished by the choice of the "main" parameter considered as a debonding criterion: local IFSS, τ_d, in the "stress-based" model, or critical energy release rate, G_{ic}, in the "energy-based" model. The stress-based model originated from one-dimensional shear-lag stress transfer analysis developed by Cox [37] but with corrected shear-lag parameter as proposed by Nayfeh [38]; its most detailed representation can be found in Ref. [11]. The energy-based model was the analytical (variational mechanics) model of the pull-out and microbond tests proposed by Nairn [12] and based on generalized fracture mechanics of composites. Both models included residual thermal stresses and interfacial friction. The main assumptions of both models were that (1) the matrix is elastic and isotropic, and the fiber is elastic and transversely isotropic; (2) the matrix droplet can be considered as a cylinder in which the fiber is co-axially embedded, and the radius of the matrix cylinder is chosen to match the total matrix volume within the embedded fiber region ("equivalent cylinder" approach [12,14]); and (3) friction in the debonded regions is constant, i.e., in terms of "interfacial frictional stress", τ_f, it is assumed that τ_f = const. As has been shown elsewhere [11,14,25,39–43], force–displacement curves modeled under these assumptions showed good agreement with experimental ones.

The basis for calculation of interfacial strength parameters for a given individual specimen is the relationship between the force, F, applied to the loaded fiber end, and the crack length, a, in the specimen at this moment. This relationship can be written in the form

$$F = F\left(a, l_e, \tau_d, \tau_f, \text{ other parameters}\right) \tag{2}$$

for the stress-based model, and

$$F = F\left(a, l_e, G_{ic}, \tau_f, \text{ other parameters}\right) \tag{3}$$

for the energy-based model. "Other parameters" include mechanical and thermal properties of the fiber and the matrix and specimen geometry. The explicit expressions for Eq. (2) and Eq. (3) are rather complicated. These are given in the Appendix: Eq. (A1) as explicit Eq. (2) and Eq. (A6) as explicit Eq. (6). The derivation of these equations can be found in Refs. [11,24,25,40].

Eqs. (2) and (3) (i.e. (A1) and (A6)) relate the force measured in the important points of the force–displacement curve (A, B, D) to the values of the interfacial strength parameters ($\{\tau_d, \tau_f\}$ or $\{G_{ic}, \tau_f\}$). For instance, within the frames of our stress-based model

$$F_d = F\left(a, l_e, \tau_d, \tau_f, \text{ other parameters}\right)\Big|_{a=0}; \tag{4}$$

$$F_b = F\left(a, l_e, \tau_d, \tau_f, \text{ other parameters}\right)\Big|_{a=l_e}; \tag{5}$$

$$F_{max} = \max_{0\le a\le l_e} F\left(a, l_e, \tau_d, \tau_f, \text{ other parameters}\right). \tag{6}$$

Explicit forms of Eqs. (4) and (5) can easily be derived from Eq. (A1). Finding the expression for F_{max} is much more complicated; its explicit form, derived in Refs. [11,23], is given in the Appendix as Eq. (A2).

For each individual specimen, the embedded length, l_e, and "other parameters" are constant, and the crack length, a, either is exactly specified (Eqs. (4) and (5)) or can easily be determined from the $F(a)$ relationship (Eq. (6)). Therefore, each of Eqs. (4)–(6) can be considered as an implicit equation in two variables, τ_d and τ_f. Similarly, starting from Eq. (3), we can derive three implicit equations with G_{ic} and τ_f as unknown values.

Since the number of Eqs. (3) is greater than the number of unknown parameters (2 in each model), the values of these parameters can be estimated by several different methods:

1). "Traditional" method. The interfacial frictional stress, τ_f, and the adhesion parameter (τ_d or G_{ic}) are determined by solving simultaneous Eqs. (4) and (6), which yield the debond force, F_d, and the peak force, F_{max}. In the stress-based model this can be done very easily, since F_d does not depend on interfacial friction and Eq. (4) becomes [11,22].

$$F_d = \frac{\pi d_f}{\beta}\left[\tau_d \tanh(\beta l_e) - \tau_T \tanh(\beta l_e)\tanh\left(\frac{\beta l_e}{2}\right)\right], \tag{7}$$

where β is the Nayfeh's shear-lag parameter [38] and τ_T is a term having dimensions of stress, which appears due to residual thermal stresses [11,14]. Thus, τ_d can be unambiguously determined from

Eq. (7). Then, substituting its value into the equation derived for F_{max} (Eq. (19) in Ref. [11] or Eq. (2) in Ref. [23]), we can calculate τ_f.

For the energy-based model, the calculation is more complicated, since in this model the debond force itself is influenced by friction [12]; both F_d and F_{max} values appeared to depend on both G_{ic} and τ_f. A rapidly converging iterative scheme for solving simultaneous Eqs. (4) and (6) for G_{ic} and τ_f has been presented in Ref. [24].

2). "Alternative" method is based on solving simultaneous Eqs. (5) and (6), i.e. on F_b and F_{max} values. Its evident advantage is that τ_f can immediately be calculated as

$$\tau_f = \frac{F_b}{\pi d_f l_e}. \quad (8)$$

Then τ_f is substituted into Eq. (6), and τ_d or G_{ic} is calculated [23,24]. The "alternative" method is often more reliable than the "traditional" one, since the "kink" in the force–displacement curve may hardly be distinguishable (which results in large error in the F_d value), while F_b can be reliably measured for most pull-out specimens. Therefore, this method can be used, e.g., for evaluation of pull-out tests on specimens with large free fiber length.

3). "Indirect" method [25,40] has been developed for pull-out experiments in which neither F_d nor F_b can be reliably determined, and the only measurable value is F_{max}. It is based on fitting the experimental $F_{max}(l_e)$ relationship by a theoretical curve (6) using a non-linear least-squares method with two fitting parameters, τ_d and τ_f (or G_{ic} and τ_f). We should note that the indirect method can yield large errors if the range of embedded lengths is not wide enough or if the number of tested specimens is small [14,24,44]. Therefore, methods based on the evaluation of individual force–displacement curves should be definitely preferred over the "indirect" approach [14,24].

The basic formulas for calculating τ_d, G_{ic}, and τ_f, as well as the definitions of intermediate parameters required for the calculation, can be found in the Appendix.

4. Results and discussion

We have performed a large number of pull-out tests for various fiber–matrix systems and calculated the local interfacial strength parameters using the methods described above in Sections 2 and 3. A part of the obtained results is presented in Table 3.

The brief analysis of these results shows that the interfacial strength parameters depend, first of all, on the chemical nature of contacting surfaces (i.e. interactions between the fiber and the matrix at the molecular level). In glass fiber – epoxy resin systems, the local IFSS for quasi-static pull-out increased by 20–40% when the fibers were sized with chemical compositions containing γ-APS, which promoted formation of chemical bonds between the fiber and the epoxy resin. This effect was repeatedly reported earlier by many researchers [30,45,46]. The effect of other factors was not so obvious; below we consider this in more detail.

4.1. Geometric factors

4.1.1. Embedded length

It is generally known that the *apparent* IFSS strongly decreases with the embedded length [4,6,11,21]. The concept of *local* interfacial shear strength [6,21,22] has been specially developed in order to find a parameter which should not depend on specimen geometry, including the embedded length. However, since the local IFSS is a statistical (random) value, real experiments may show a correlation between τ_d and l_e. This can be illustrated, e.g., by Fig. 5a and b, in which the local IFSS for the system glass fiber – epoxy resin with HY 917 hardener is plotted *versus* the embedded length. For unsized fibers (Fig. 5a), τ_d values are distributed mainly between 40 and 100 MPa, with a small apparent increase with l_e. For sized fibers (Fig. 5b), the τ_d values for short embedded lengths are very large (up to 220 MPa) and practically irreproducible (the local IFSS values for two specimens with close l_e can differ appreciably). And in general, τ_d values tend to decrease with l_e in this case. This behavior can be explained if we analyze the patterns of specimen failure. For sized fibers (high adhesion to epoxy resin), a small part of matrix meniscus (wetting cone) can often be found on the fiber after the pull-out completion. Since the size of this residual meniscus part is different for different specimens, the values of the force required for meniscus fracture (and thus for completed fiber pull-out) are also very different, which results in large scatter in the calculated τ_d values. The effect of meniscus is especially pronounced for short embedded lengths, when the force required for meniscus break is comparable to the interfacial adhesion force or even exceeds it. With increasing l_e, the relative part of the meniscus break force obviously decreases, and, as a result, the calculated τ_d values also virtually decrease (see Fig. 5b). It should be mentioned that the range of anomalous τ_d behavior in Fig. 5b is limited to the embedded lengths up to 30–40 μm, which corresponds to only 2–4 fiber diameters. As was noted in the literature [4,6,10], the shear-lag theory, on which the τ_d determination in our model is based, may not be valid if the aspect ratio l_e/d_f is less than 4–5 fiber diameters. This is an additional source of errors. Therefore, in this paper we discarded all results obtained for specimens with $l_e < 40$ μm.

For specimens with unsized fibers (moderate adhesion to epoxy resin), the fiber was typically pulled out of the resin without

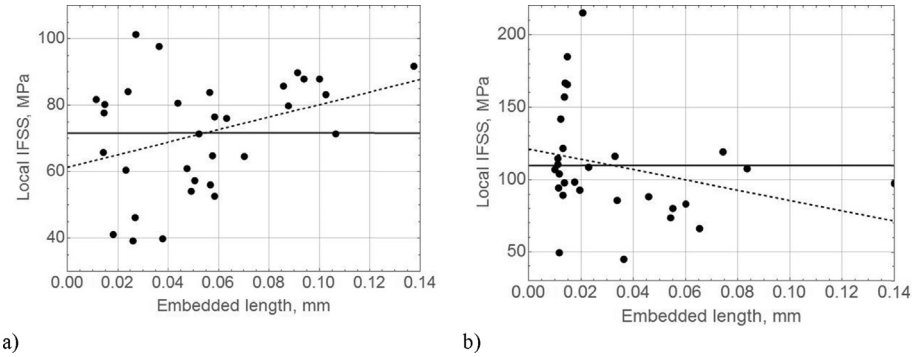

Fig. 5. Plots of local IFSS in the system of glass fiber and epoxy resin with HY 917 hardener *versus* the embedded length: a) unsized fiber; b) sized fiber. Filled circles present experimental points; dashed line — linear fit; full line — mean value.

meniscus fracture, and the calculated τ_d values did not decrease with the embedded length (Fig. 5a). Nevertheless, for this specimen set we discarded the results for specimens with $l_e < 40$ μm as well. All our experience, including this paper, evidenced that for $l_e > (4…5)\, d_f$ the local IFSS calculated using our approach can be considered as approximately constant.

4.1.2. Size and shape of the matrix droplet

In all pull-out tests in this paper the shape of the matrix droplet was close to hemispherical. However, the droplet diameter at the pull-out test installation at the IPF was 2.5 mm, and at the BAM, 1.0 mm. The comparison of the results obtained for the same fiber–matrix pairs at the same conditions (strings F and BAM in Table 3) shows that the calculated values of the local interfacial strength parameters are practically identical.

Eqs. (A1–A18) for calculating the local IFSS and the critical energy release rate in the "equivalent cylinder" approximation [12,23] include the values of V_f and V_m, the fiber and matrix volume fractions within the "reinforced" specimen part, which, in turn, depend on the droplet shape, fiber diameter, and embedded length. Therefore, it is extremely important to know the droplet shape as more accurately as possible. For hemispherical droplets, the formula $V_f = V_f(l_e, D_m, d_f)$, where D_m is the matrix droplet diameter, was presented in Ref. [11]. It should be noted that in real pull-out specimens the droplet shape may differ from a hemisphere (spherical segment, cuboid brick, prism or even more intricate shape). In the case of a spherical segment, for correct V_f calculation one should take not the radius or diameter of a contact region with the substrate or holder, but the radius of curvature of the droplet surface near the fiber entry point. For small droplets, the latter is equal to the radius of the matrix sphere and can be calculated from the droplet height and the diameter of the contact spot using trigonometric equations [47].

4.1.3. Free fiber length

The effect of the free fiber length on the pull-out test was briefly discussed in the Introduction. With the increase in l_{fr}, compliance of the experimental installation also increases. As a result, the shape of the recorded force–displacement curve changes, and its characteristic points, such as the debond point (A), become ever less discernible. For *very* large l_{fr}, after reaching the maximum force value (F_{max}, point B) the force–displacement curve jumps over the segment of instable debonding, so that even the position of point D may become uncertain. Thus, the advantages of "stress-controlled" pull-out vanish completely; in such experimental configuration, only the peak force, F_{max}, and the apparent IFSS, τ_{app}, can be measured.

4.2. Thermodynamic and kinetic factors

The effect of thermodynamic and kinetic factors (thermal history, humidity, loading rate) was also mentioned in Section 1 (Introduction). Of course, the most important thermodynamic factor is "by default" chemical nature of the matrix and the fiber surface which determines interfacial interactions at the molecular level; all others can be regarded as a kind of "modifier". As can be seen in Table 3, γ-APS sized glass fibers in all cases showed higher adhesion to epoxy resins than unsized fibers. As other thermodynamic and kinetic factors are concerned, in this paper we only could estimate the effect of displacement rate on the local interfacial strength parameters. Table 3 (strings S and F/BAM) shows that the increase in the displacement rate by two orders of magnitude resulted in only minor increment in τ_d and G_{ic} values (for most fiber–matrix pairs, within the margin of error; for γ-APS sized glass fiber + epoxy resin with HY 917 hardener, up to 30%). Thus, we can consider the results of the pull-out tests at these displacement rates (0.01 and 1 μm/s) as very close. The advantage of the higher displacement rate is shorter time required for the measurement; however, the smaller displacement rate yields more detailed shapes of force–displacement curves, which results in higher accuracy (see also Subsection 4.3.4). A marked difference of the measured interfacial strength parameters in a pull-out test can be only expected if the displacement rates differ by 5–6 orders of magnitude [44].

4.3. Data reduction

4.3.1. "Stress-based" and "energy-based" models

These two groups of models are distinguished by the parameter which is chosen as a debonding criterion (τ_d or G_{ic}) and, at first sight, are mutually exclusive. For a long time, there was a discussion in the literature which of these criteria is the "true" one. However, it was shown [29], that G_{ic} and τ_{app} for an individual specimen in some cases are related by an algebraic equation. As a result, τ_d and G_{ic} are also functionally related. In the models which we use for interfacial strength parameters calculation [11,12,24,25,40], G_{ic} is proportional to τ_d^2 in the absence of thermal shrinkage and interfacial friction. In general case, the relationship is more complicated but also can be expressed by relatively simple algebraic equations. In practice, this kind of relationship between the local IFSS and the critical energy release rate means that τ_d and G_{ic} are symbatic parameters, and for two different fiber–matrix pairs the G_{ic} values differ more than τ_d. Our results are in agreement with this conclusion (see Table 3, column G_{ic}).

4.3.2. "Traditional" and "alternative" methods of calculation of interfacial strength parameters

Table 4 presents the local IFSS (τ_d) and interfacial frictional stress (τ_f) values calculated for several fiber–matrix specimen sets using different methods described in Section 3. Each set included 12–16 pull-out specimens. The "traditional" method was based on τ_d determination from the debond force value, F_d, at the kink point A (see Fig. 2) and following τ_f calculation from the maximum force, F_{max} (point B). In the "alternative" method, the interfacial frictional stress, τ_f, was first calculated from the post-debond force value, F_b (point D, Eq. (8)), and then τ_d was determined from the maximum force, F_{max}. The approach marked as "FIMATEST" was a kind of "hybrid" of these two methods: the local IFSS was determined from the kink force similarly to the traditional method, and the interfacial frictional stress, from the post-debond force, as in the "alternative" method. We should emphasize an important difference in

Table 4
Comparison of local adhesion parameters obtained by IPF and Textechno (FIMATEST) and calculated using different approaches.

System	Specimen set No.	Local IFSS/Frictional stress, MPa		
		Traditional	Alternative	FIMATEST
GF + RIM epoxy	1	50.30/—*	76.38/16.97	55.51/12.22
	2	57.29/—	92.30/15.16	63.11/9.97
	3	48.90/—	59.55/4.67	n/a
	4	56.97/—	79.87/10.94	n/a
	5	60.73/—	91.71/—	n/a
CF + PA 6,6	1	51.68/—	104.64/13.47	61.92/9.74
	2	39.44/24.62	70.52/9.87	56.64/8.56
	3	44.93/27.50	78.01/6.40	58.99/5.62
	4	45.20/—	78.88/11.47	56.89/12.82
	5	46.96/—	86.38/6.96	n/a
	6	45.03/—	76.53/10.18	n/a
	7	65.72/—	111.86/6.16	n/a

* Indeterminate: calculated $\tau_f > \tau_d$, which is impossible.

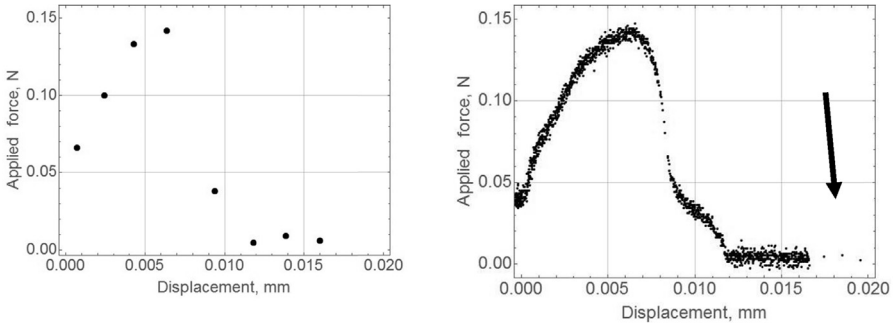

Fig. 6. Model force–displacement curves recorded at different displacement speed (v_d) and acquisition rate (f_{ac}): a) $v_d = 0.01$ μm/s, $f_{ac} = 0.01$ s^{-1}; b) $v_d = 0.01$ μm/s (1 μm/s in the post-debonding segment marked by the arrow), $f_{ac} = 1$ s^{-1}.

the determination of the debond force value, F_d, in the "traditional" and FIMATEST approaches. In the traditional approach, the F_d value was taken at the point in which the force–displacement curve began to deviate from a straight line (point *A* in Fig. 2). In the FIMATEST approach, two tangent lines were drawn at two successive segments of the force–displacement curve, and the F_d value was taken at the point of their intersection (A_1). Thus, the measured debond forces, and, as a consequence, the calculated local IFSS values, were greater for the FIMATEST approach than for the "traditional" one. All values presented in the FIMATEST column in Table 4 were obtained using the FIMATEST system [30] developed by Textechno. Then the same raw data (force–displacement curves) were evaluated using the "traditional" and "alternative" approaches in the *Mathematica*® programming environment [32]. Other specimen sets were tested on the IPF lab equipment [31,32] and then evaluated using *Mathematica*.

The most striking result obtained in our tests was that in the traditional approach it appeared that for most specimens the experimentally measured peak force, F_{max}, could be only reached if $\tau_f > \tau_d$ (!) Since this is physically impossible (for this behavior, F_b should be greater than F_{max}), we concluded that the behavior of force–displacement curves in their rising part can be much more complicated than is shown in (simplified) Fig. 2. One of the most important factors affecting force–displacement curves is the specimen shape [48,49]. Other possible reasons are discussed, e.g., in Ref. [50]. In any case, the uncertainty in the F_d value is very large, and therefore the "alternative" method which does not use the debond force seems to be much better. The τ_d values calculated using this method (see Table 4) are rather large but still reasonable, and the interfacial frictional stress, τ_f, corresponds well to the frictional stress after debonding. Similar τ_f values were obtained using the FIMATEST method, since the F_b value was measured by a similar procedure. The local IFSS calculated in this approach is obviously higher than in the "traditional" one (see Table 4 and Fig. 2) but much smaller than τ_d from the alternative test. Note that if we calculate the peak force, F_{max}, according to Eq. (A2) using τ_d and τ_f determined using the FIMATEST procedure, it will be considerably smaller than experimental F_{max} value. This can be regarded as a deficiency of the method, since F_{max} is experimentally measured with the highest accuracy of all characteristic points of a force–displacement curve.

Table 3 shows similar relations between local IFSS values determined using the traditional (τ_{d1}) and alternative (τ_{d2}) approaches. Note also that the interfacial frictional stress values from the traditional method (τ_{f1}) are highly overestimated.

4.3.3. "Indirect" method

When this approach was proposed [25,40], it seemed to be a good tool for determining τ_d and τ_f from solely F_{max} values measured over a wide range of embedded lengths. In practice, however, it appeared to be not very accurate, especially regarding the τ_f values to be determined. Though it often yields a quite plausible value of the local IFSS (close to τ_d obtained using the alternative method), it absolutely cannot give a reasonable τ_f estimation. This can be illustrated by the last two columns in Table 3. In any case, methods based on individual force–displacement curves should be preferred.

4.3.4. Pull-out data recording

An unexpected problem arose during evaluation of some force–displacement curves recorded in the pull-out test. If the displacement velocity was high enough and the acquisition rate was very low, the resulting "curve" appeared to be composed of a set of distantly spaced points (Fig. 6a), and its detailed shape could not be recovered. In particular, the current force values at all three important points (F_d, F_b and even F_{max}) could be only determined with large errors; also a large error was inherent in the measured embedded length, l_e (not shown in Fig. 6a). On the contrary, for quasi-static pull-out and sufficiently large acquisition rate, the force–displacement curve was recorded with high resolution; it can be used for accurate measurement of all characteristic forces and, in addition, for visualization of the instrumental error (Fig. 6b). We recommend using such test equipment settings that the significant part of the force–displacement curve (up to point *D*) should include *several hundred* experimental points. At the same time, after debonding completion at point *D* the displacement velocity can be increased considerably in order to shorten the time till the full fiber pull-out (right side of the plot in Fig. 6b, marked by an arrow).

5. Conclusion

Experimental results of our pull-out tests on several fiber–polymer matrix systems showed that the values of local interfacial strength parameters (local IFSS, critical energy release rate) weakly depended on geometrical factors. This is not surprising, since the local parameters were specially introduced so as to exclude the effects of the specimen shape. On the other hand, the pull-out test appeared to be sensitive to physical factors, such as fiber sizing and displacement rate. A very important issue is the choice of an adequate method of data reduction (analysis of experimental force–displacement curves). After having compared several methods of determination of the local interfacial strength parameters, we recommend to calculate the τ_d and G_{ic} values using the "alternative" method, i.e. from the maximum force recorded in a pull-out test and the interfacial frictional force immediately after fiber debonding.

Conflict of interest

The authors declare an absence of conflicts of interest.

Acknowledgement

The authors are thankful to Martina Bistritz, Steffi Preßler and Alma Rothe for technical support.

Appendix

Below are presented the basic formulas for calculating the interfacial strength parameters, as well as the expressions for intermediate parameters and coefficients required for the calculation.

Stress-based approach

Applied force as a function of the crack length [11,40]:

$$F(a)=\frac{\pi d_f}{\beta}\left\{\tau_d\tanh[\beta(l_e-a)]-\tau_T\tanh[\beta(l_e-a)]\tanh\left[\frac{[\beta(l_e-a)]}{2}\right]+\beta a\tau_f\right\}. \tag{A1}$$

Maximum force in a pull-out test as a function of the embedded length [11,23]:

$$F_{\max}(l_e)=\begin{cases}\dfrac{\pi d_f}{\beta}\left[\tau_d\tanh(\beta l_e)-\tau_T\tanh(\beta l_e)\tanh\left(\dfrac{\beta l_e}{2}\right)\right], & \beta l_e<\ln\left(u+\sqrt{u^2+1}\right);\\ \dfrac{\pi d_f}{\beta}\left\{\tau_d\dfrac{u}{\sqrt{u^2+1}}-\tau_T\left(1-\dfrac{1}{\sqrt{u^2+1}}\right)+\tau_f\left[\beta l_e-\ln\left(u+\sqrt{u^2+1}\right)\right]\right\}, & \beta l_e\geq\ln\left(u+\sqrt{u^2+1}\right),\end{cases} \tag{A2}$$

where

$$\beta^2=\frac{8}{d_f^2E_AE_m}\left[\frac{E_AV_f+E_mV_m}{\frac{V_m}{4G_A}+\frac{1}{2G_m}\left(\frac{1}{V_m}\ln\frac{1}{V_f}-1-\frac{V_f}{2}\right)}\right] \tag{A3}$$

is the Nayfeh's shear-lag parameter [34];

$$\tau_T=\frac{\beta d_fE_A}{4}(\alpha_A-\alpha_m)\Delta T \tag{A4}$$

is a term having dimensions of stress, which appears due to residual thermal stresses [36];

$$u=\frac{\sqrt{\tau_T^2+4\tau_f\left(\tau_d-\tau_f\right)}-\tau_T}{2\tau_f} \tag{A5}$$

is a dimensionless parameter characterizing the stress transfer in a pull-out specimen [11]; E_A is the axial tensile modulus of the fiber, E_m is the tensile modulus of the matrix, G_A is the longitudinal shear modulus of the fiber, G_m is the shear modulus of the matrix, α_A is the axial coefficient of thermal expansion (CTE) of the fiber, α_m is the CTE of the matrix, ΔT is the difference between the test temperature and the reference stress-free temperature, and V_f and V_m are the fiber and matrix volume fractions within the "reinforced" specimen part.

Energy-based approach

Applied force as a function of the crack length [24]:

$$F(a)=\frac{\pi d_f^2}{4}\left[-\frac{c_1(a)}{2c_2(a)}+\sqrt{\left(\frac{c_1(a)}{2c_2(a)}\right)^2-\frac{c_0(a)-G_{ic}}{c_2(a)}}\right], \tag{A6}$$

where [12,24,25].

$$c_0(a)=\frac{d_f}{4}\left\{C_{33s}k^2a^2-2D_{3s}ka\Delta T+\left(\frac{D_3^2}{C_{33}}+\frac{V_m(\alpha_T-\alpha_m)^2}{V_fA_0}\right)(\Delta T)^2-D_{3s}\Delta T\left[kC_T(a)+\left(ka-\frac{D_3\Delta T}{C_{33}}\right)C_T'(a)\right]\right\}; \tag{A7}$$

$$c_1(a)=\frac{d_f}{4}\left\{(2+C_T'(a))D_{3s}\Delta TA_6-2C_{3s}A_6ka-\frac{V_f}{2}\left(\frac{1}{E_A}-\frac{1}{E_m}\right)\times\left[kC_T(a)+\left(ka-\frac{D_3\Delta T}{C_{33}}\right)C_T'(a)\right]\right\}; \tag{A8}$$

$$c_2(a)=\frac{d_f}{4}\left\{C_{33s}A_6^2+\frac{V_f}{2}\left(\frac{1}{E_A}-\frac{1}{E_m}\right)A_6C'_T(a)\right\}; \tag{A9}$$

$$A_6=\frac{V_mE_m}{V_fE_A+V_mE_m}; \tag{A10}$$

$$C_{33s}=\frac{1}{2}\left(\frac{1}{E_A}+\frac{V_f}{V_mE_m}\right); \tag{A11}$$

$$C_{33}=C_{33s}-\frac{V_mA_3^2}{V_fA_0}; \tag{A12}$$

$$D_{3s}=\frac{1}{2}(\alpha_A-\alpha_m), \tag{A13}$$

$$D_3=D_{3s}-\frac{V_mA_3}{V_fA_0}(\alpha_T-\alpha_m); \tag{A14}$$

$$A_0=\frac{V_m(1-\nu_T)}{V_fE_T}+\frac{1-\nu_m}{E_m}+\frac{1+\nu_m}{V_fE_m}; \tag{A15}$$

$$A_3=-\left(\frac{\nu_A}{E_A}+\frac{V_f\nu_m}{V_mE_m}\right); \tag{A16}$$

$$C_T(a)=\frac{1}{\beta}\tanh\frac{\beta(l_e-a)}{2}; \tag{A17}$$

$$C_T'(a)=-\frac{1}{2}sech^2\frac{\beta(l_e-a)}{2}; \tag{A18}$$

$k = 4\tau_f/d_f$ is the frictional stress transfer rate, E_T is the transverse tensile modulus of the fiber, α_T is the transverse CTE of the fiber, ν_A and ν_T are respectively the axial and transverse Poisson ratios of the fiber, and ν_m is the Poisson ratio of the matrix.

References

[1] G.V. Shiriajeva, G.D. Andreevskaya, Method of determination of the adhesion of resins to the surface of glass fibers, Plast. Massy (Polym. Compd. USSR) 4 (1962) 42–43.
[2] L.S. Penn, E.R. Bowler, A new approach to surface energy characterization for adhesive performance prediction, Surf. Interface Anal. 3 (1981) 161–164.
[3] J.P. Favre, J. Perrin, Carbon fibre adhesion to organic matrices, J. Mater. Sci. 7 (1972) 1113–1118.
[4] G. Désarmot, J.P. Favre, Advances in pull-out testing and data analysis, Compos. Sci. Technol. 42 (1991) 151–187.
[5] M.R. Piggott, Failure processes in the fibre-polymer interphase, Compos. Sci. Technol. 42 (1991) 57–76.
[6] Y.A. Gorbatkina, Adhesive Strength of Fiber-polymer Systems, Ellis Horwood, New York, 1992.
[7] H.J. Jacobasch, K. Grundke, P. Uhlmann, F. Simon, E. Mäder, Comparison of surface-chemical methods for characterizing carbon fiber–epoxy resin composites, Compos. Interface 3 (1996) 293–320.
[8] M.J. Pitkethly, J.P. Favre, U. Gaur, J. Jakubowski, S.F. Mudrich, D.L. Caldwell, L.T. Drzal, M. Nardin, H.D. Wagner, L. Di Landro, A. Hampe, J.P. Armistead, M. Desaeger, I. Verpoest, A robin-round programme on interfacial test methods, Compos. Sci. Technol. 48 (1993) 205–214.
[9] B. Miller, P. Muri, L. Rebenfeld, A microbond method for determination of the shear strength of a fiber–resin interface, Compos. Sci. Technol. 28 (1987) 17–32.
[10] C.H. Liu, J.A. Nairn, Analytical fracture mechanics of the microbond test including the effects of friction and thermal stresses, Int. J. Adhesion Adhes. 19 (1999) 59–70.
[11] S. Zhandarov, E. Mäder, Peak force as function of the embedded length in the pull-out and microbond tests: effect of specimen geometry, J. Adhes. Sci. Technol. 19 (2005) 817–855.
[12] J.A. Nairn, Analytical fracture mechanics analysis of the pull-out test including the effects of friction and thermal stresses, Adv. Compos. Lett. 9 (2000) 373–383.
[13] D.B. Marshall, W.C. Oliver, Measurement of interfacial mechanical properties in fiber-reinforced ceramic composites, J. Am. Ceram. Soc. 70 (1987) 542–548.
[14] S. Zhandarov, E. Mäder, Characterization of fiber/matrix interface strength: applicability of different tests, approaches and parameters, Compos. Sci. Technol. 65 (2005) 149–160.
[15] D.M. Rein, L.M. Beder, V.G. Baranov, A.S. Chegolya, The model of polymer crystallization under non-isothermal conditions, Acta Polym. 32 (1981) 1–5.
[16] C.A. Fuentes, K.W. Ting, C. Dupont-Gillain, M. Steensma, A.G. Talma, R. Zuijderduin, A.W. Van Vuure, Effect of humidity during manufacturing on the interfacial strength of non-pre-dried flax fibre/unsaturated polyester composites, Compos. A 84 (2016) 209–215.
[17] M. Lebbai, J.K. Kim, M.M.F. Yuen, Effects of moisture and elevated temperature on reliability of interfacial adhesion in plastic packages, J. Electron. Mater. 32 (2003) 574–582.
[18] K.A. Downes, J.L. Thomason, A method to measure the influence of humidity and temperature on the interfacial adhesion in polyamide composites, Compos. Interface 22 (2015) 757–766.
[19] S.N. Zhurkov, Das Problem der Festigkeit fester Körper, Z. Phys. Chem. 231 (1960) 183–190.
[20] S.N. Zhurkov, Kinetic concept of the strength of solids, Int. J. Fract. 26 (1984) 295–307.
[21] L.B. Greszczuk, Theoretical studies of the mechanisms of the fibre–matrix interface, in: Interfaces in Composites, ASTM STP 452, American Society for Testing and Materials, Philadelphia, PA, 1969, pp. 42–48.
[22] S.F. Zhandarov, E.V. Pisanova, The local bond strength and its determination by the fragmentation and pull-out tests, Compos. Sci. Technol. 57 (1997) 957–964.
[23] S. Zhandarov, E. Mäder, An alternative method of determining the local interfacial shear strength from force–displacement curves in the pull-ou tand microbond tests, Int. J. Adhesion Adhes. 55 (2014) 37–42.
[24] S. Zhandarov, E. Mäder, Determining the interfacial toughness from force–displacement curves in the pull-out and microbond tests using the alternative method, Int. J. Adhesion Adhes. 65 (2016) 11–18.
[25] S. Zhandarov, E. Mäder, Indirect estimation of fiber/polymer bond strength and interfacial friction from maximum load values recorded in the microbond and pull-out tests. Part II: critical energy release rate, J. Adhes. Sci. Technol. 17 (2003) 967–980.
[26] Y. Wang, J.G. Williams, Dynamic crack growth in TDCB specimens, Int. J. Mech. Sci. 38 (1996) 1073–1088.
[27] D. Bruno, F. Greco, P. Lonetti, Dynamic Mode I and Mode II crack propagation in fiber reinforced composites, Mech. Adv. Mater. Struct. 16 (2009) 442–455.
[28] M.F. Funari, F. Greco, P. Lonetti, R. Luciano, R. Penna, An interface approach based on moving mesh and cohesive modeling in Z-pinned composite laminates, Composites Part B 135 (2018) 207–217.
[29] S. Zhandarov, E. Pisanova, B. Lauke, Is there any contradiction between the stress and energy failure criteria in micromechanical tests? Part I. Crack initiation: stress-controlled or energy-controlled? Compos. Interfac. 5 (1998) 387–404.
[30] E. Mäder, S.L. Gao, R. Plonka, J. Wang, Investigation on adhesion, interphases, and failure behaviour of CBT/glass fiber composites, Compos. Sci. Technol. 67 (2007) 3140–3150.
[31] W. Jenschke, D. Arnold, E. Mäder, Anlage zur Herstellung von Einzelfaser-Modellverbunden, http://www.ipfdd.de/frameset.html?/research/equip/equipment.html.
[32] E. Mäder, K. Grundke, H.J. Jacobasch, G. Wachinger, Surface, interphase and composite property relations in fibre-reinforced composites, Composites 25 (1994) 739–744.
[33] E. Maeder, U. Moerschel, M. Effing, Quality assessment of composites, JEC Compos. Mag. 102 (2016) 49–51.
[34] Textechno H. Stein GmbH & Co. KG, Moenchengladbach, Fibre-Matrix Adhesion Tester FIMATEST, http://www.textechno.com/product/fimatest, 2017-05-05.
[35] A. Hampe, G. Kalinka, S. Meretz, E. Schulz, An advanced equipment for single-fibre pull-out designed to monitor the fracture process, Compos. A 26 (1995) 40–46.
[36] Wolfram Language & System Documentation Center, http://reference.wolfram.com/language/.
[37] H.L. Cox, The elasticity and strength of paper and other fibrous materials, Br. J. Appl. Phys. 3 (1952) 72–79.
[38] A.H. Nayfeh, Thermomechanically induced interfacial stresses in fibrous composites, Fibre Sci. Technol. 10 (1977) 195–209.
[39] E. Pisanova, S. Zhandarov, E. Mäder, I. Ahmad, R.J. Young, Three techniques of interfacial bond strength estimation from direct observation of crack initiation and propagation in polymer–fibre systems, Compos. A 32 (2001) 435–443.
[40] S.F. Zhandarov, E. Mäder, O.R. Yurkevich, Indirect estimation of fiber/polymer bond strength and interfacial friction from maximum load values recorded in the microbond and pull-out tests. Part I: local bond strength, J. Adhes. Sci. Technol. 16 (2002) 1171–1200.
[41] M.C. Andrews, D.J. Bannister, R.J. Young, Review: the interfacial properties of aramid/epoxy model composites, J. Mater. Sci. 31 (1996) 3893–3913.
[42] S. Zhandarov, E. Pisanova, E. Mäder, J.A. Nairn, Investigation of load transfer between the fiber and the matrix in pull-out tests with fibers having different diameters, J. Adhes. Sci. Technol. 15 (2001) 205–222.
[43] S. Zhandarov, E. Pisanova, K. Schneider, Fiber-stretching test: a new technique for characterizing the fiber–matrix interface using direct observation of crack initiation and propagation, J. Adhes. Sci. Technol. 14 (2000) 381–398.
[44] C. Scheffler, S. Zhandarov, W. Jenschke, E. Mäder, Poly (vinyl alcohol) fiber reinforced concrete: investigation of strain rate dependent interphase behavior with single fiber pullout test under quasi-static and high rate loading, J. Adhes. Sci. Technol. 27 (2013) 385–402.
[45] E. Feresenbet, D. Raghavan, G.A. Holmes, The influence of silane coupling agent composition on the surface characterization of fiber and on fiber–matrix interfacial shear strength, J. Adhes. 79 (2003) 643–665.
[46] R.-C. Zhuang, T. Burghardt, E. Mäder, Study on interfacial adhesion strength of single glass fibre/polypropylene model composites by altering the nature of the surface of sized glass fibres, Compos. Sci. Technol. 70 (2010) 1523–1529.
[47] A.D. Zimon, Adhesion of Liquids and Wetting, Chemistry, Moscow, 1974.
[48] S. Zhandarov, E. Mäder, Analysis of a pull-out test with real specimen geometry. Part I: matrix droplet in the shape of a spherical segment, J. Adhes. Sci. Technol. 27 (2013) 430–465.
[49] S. Zhandarov, E. Mäder, Analysis of a pull-out test with real specimen geometry. Part II: the effect of meniscus, J. Adhes. Sci. Technol. 28 (2014) 65–84.
[50] S. Zhandarov, C. Scheffler, E. Mäder, U. Gohs, Three specimen geometries and three methods of data evaluation in single fiber pull-out tests, Mech. Compos. Mater. (2018) (accepted for publication).